

Electronic Supplementary Material

Multi-functional layered double hydroxides supported by nanoporous gold towards overall hydrazine splitting

Yongji Qin¹, Huijie Cao^{2,3}, Qian Liu⁴, Shaoqing Yang¹, Xincai Feng¹, Hao Wang⁵, Meiling Lian⁶, Dongxing Zhang¹, Hua Wang¹, Jun Luo (✉)¹, Xijun Liu (✉)³

1 ShenSi Lab, Shenzhen Institute for Advanced Study, University of Electronic Science and Technology of China, Shenzhen 518110, China

2 Institute for New Energy Materials and Low-Carbon Technologies, School of Materials Science and Engineering, Tianjin University of Technology, Tianjin 300384, China

3 State Key Laboratory of Featured Metal Materials and Life-cycle Safety for Composite Structures, Guangxi Key Laboratory of Processing for Non-ferrous Metals and Featured Materials, School of Resources, Environment and Materials, Guangxi University, Nanning 530004, China

4 Institute for Advanced Study, Chengdu University, Chengdu 610106, China

5 China National Coal Group Corporation, Beijing 100120, China

6 Tianjin Engineering Research Center of Civil Aviation Energy Environment and Green Development, School of Transportation Science and Engineering, Civil Aviation University of China, Tianjin 300300, China

E-mails: jluo@uestc.edu.cn (Luo J); xjliu@gxu.edu.cn (Liu X)

Experimental section

1. Chemicals

Cobalt nitrate hexahydrate ($\text{Co}(\text{NO}_3)_2 \cdot 6\text{H}_2\text{O}$, $\geq 99.0\%$), cobalt acetate tetrahydrate ($\text{Co}(\text{OAc})_2 \cdot 4\text{H}_2\text{O}$, $\geq 98.0\%$), 2-methylimidazole (2-MIM, $\geq 98.0\%$) and potassium hydroxide (KOH) ($\geq 85\%$) were purchased from Shanghai Aladdin Biochemical Technology Co. Ltd. Ferric nitrate nonahydrate ($\text{Fe}(\text{NO}_3)_3 \cdot 9\text{H}_2\text{O}$, $\geq 98.0\%$), cupric nitrate trihydrate ($\text{Cu}(\text{NO}_3)_2 \cdot 3\text{H}_2\text{O}$, $\geq 98.0\%$), nickel nitrate hexahydrate ($\text{Ni}(\text{NO}_3)_2 \cdot 6\text{H}_2\text{O}$, $\geq 98.0\%$), nitric acid (HNO_3 , 65.0 ~ 68.0%), hydrochloric acid (HCl, 36.0 ~ 38.0%), hydrazine hydrate ($\text{N}_2\text{H}_4 \cdot \text{H}_2\text{O}$, 85%) and ethanol (EtOH, $\geq 99.7\%$) were obtained from Sinopharm Chemical Reagent Co., Ltd. Iridium oxide (IrO_2 , $\geq 98.0\%$) was received from Shanghai Haohong Biomedical Technology Co., Ltd. Platinum on carbon (Pt/C, 20 wt%) was acquired from Shanghai Hesen Electric Co., Ltd. Nafion solution (Dupont D520, 5wt%) was purchased from Shanghai Macklin Biochemical Technology Co., Ltd. Hexadecyl trimethyl ammonium bromide (CTAB, $\geq 99.0\%$) was obtained from Beijing Innochem Science & Technology Co., Ltd. Gold-based alloy foil (Au, 50 wt%) was received from Nanjing Yongbo metal materials Co., Ltd.

2. Characterizations

The morphology and structure were recorded by transmission electron microscope (TEM, JEM-2100 plus) and scanning electron microscope (SEM, Hitachi S-4800). The X-ray diffraction (XRD) patterns were characterized by Rigaku SmartLab 9KW. The high-angle annular dark-field scanning TEM (HAADF-STEM) and elemental mapping images were taken on a spherical probe corrected TEM (JEOL Arm200). The X-ray photoelectron spectroscopy (XPS) was carried out on Thermo Fisher Scientific ESCALAB 250Xi, and the XPS results were calibrated using C 1s (284.8 eV) data.

Figures

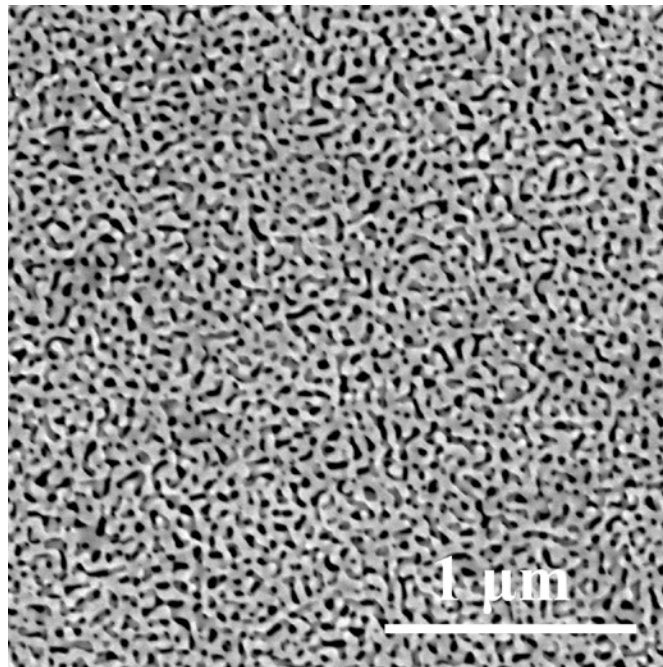


Figure S1. The SEM image of the NPG.

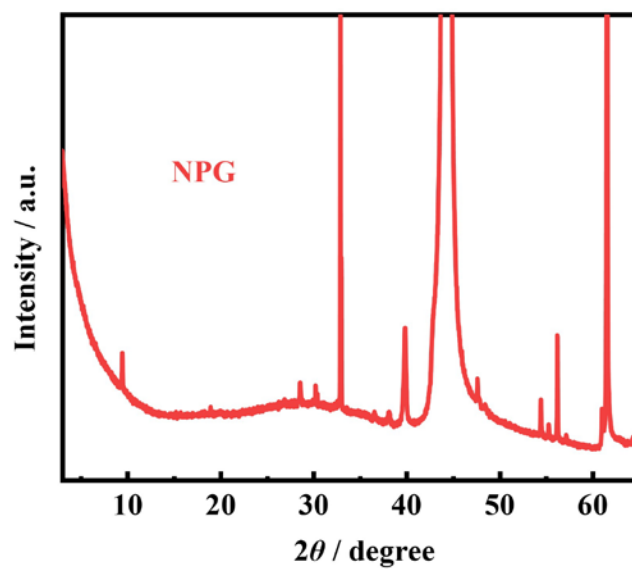


Figure S2. The XRD pattern of the NPG.

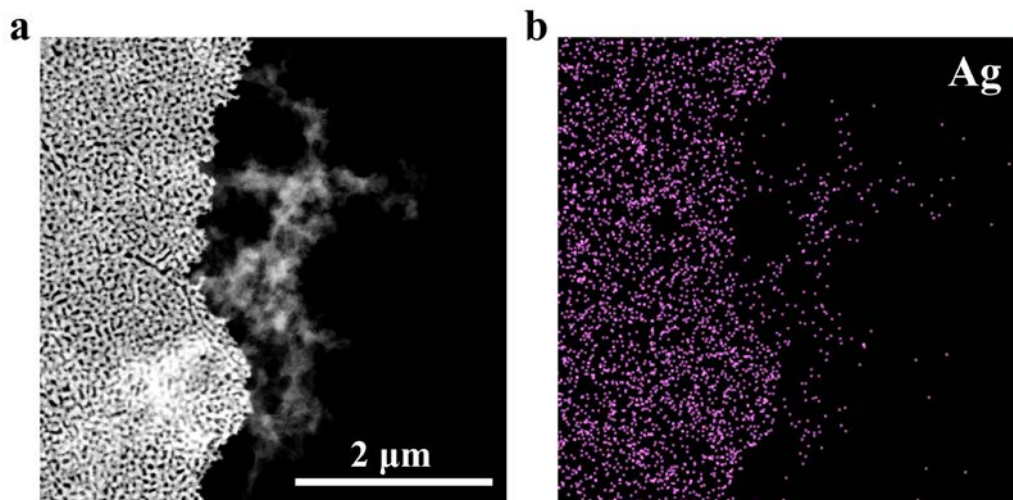


Figure S3. The HAADF-STEM image (a) and elemental mapping of Ag (b) of the NPG-HS-LDH.

Table S1. Atomic concentration (at%) of each element presented in the elemental mapping images of the NPG-HS-LDH.

| | | Atomic concentration (%) through elemental mapping test | | | | | | | |
|---------|------|---|------|-------|-------|------|-------|----|------|
| Element | Ni | Co | Fe | Cu | C | N | O | Au | Ag |
| Value | 1.69 | 4 | 1.18 | 24.15 | 31.87 | 1.65 | 25.34 | 10 | 0.11 |

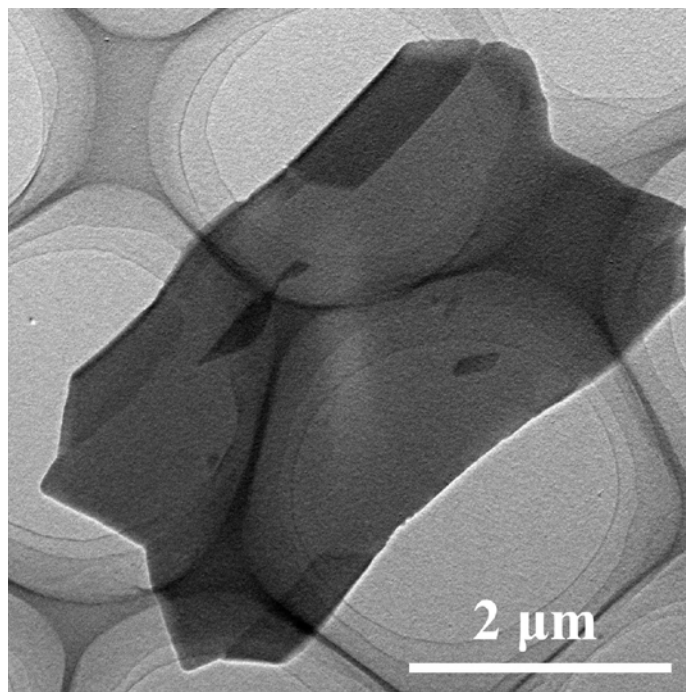


Figure S4. The TEM image of the HS-ZIF-67.

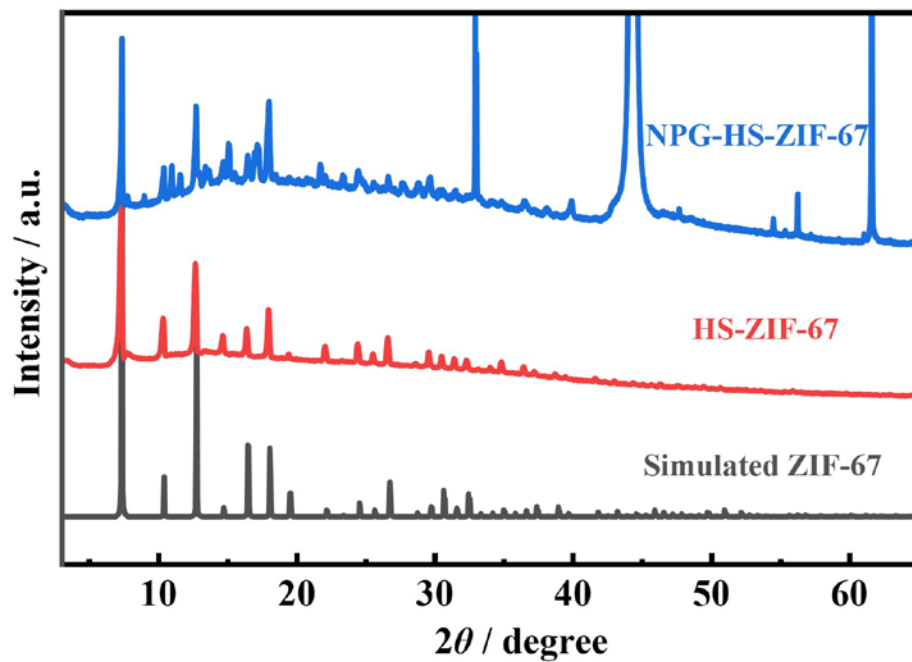


Figure S5. The XRD patterns of the NPG-ZIF-67, HS-ZIF-67 and simulated data.

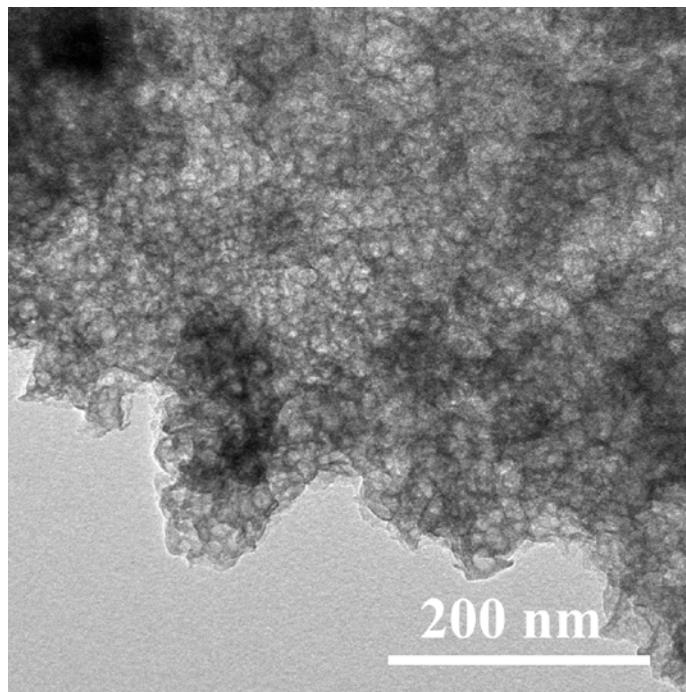


Figure S6. The TEM image of the HS-LDH.

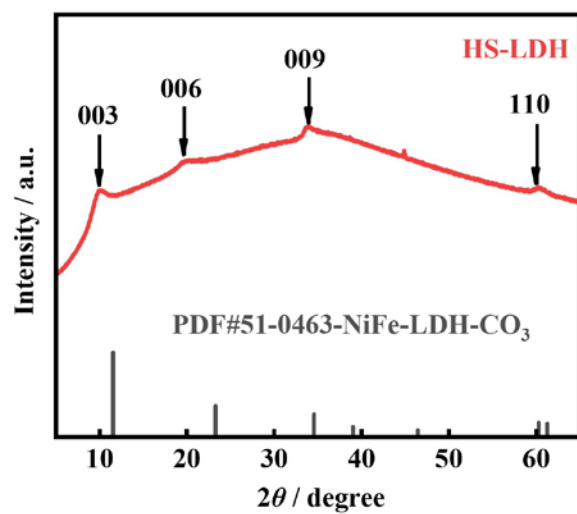


Figure S7. The XRD pattern of the HS-LDH.

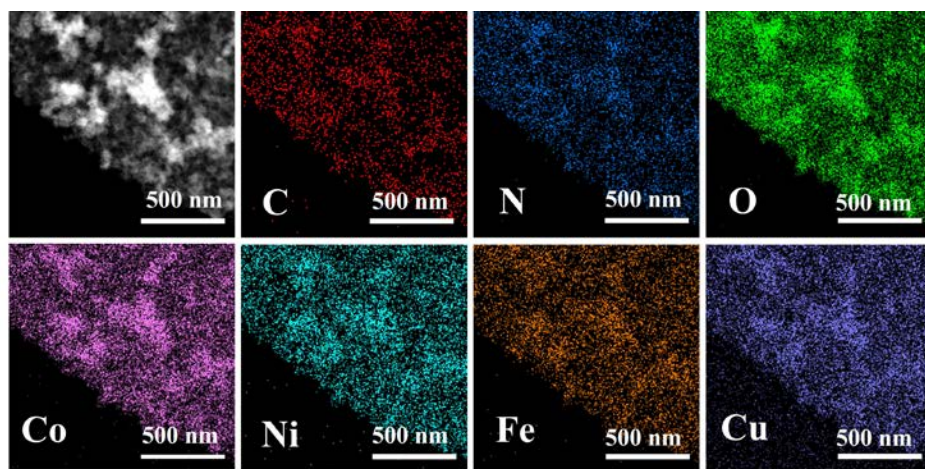


Figure S8. The HAADF-STEM and elemental mapping images of the HS-LDH.

Table S2. Atomic concentration (at%) of each element presented in the XPS survey spectrum of the NPG-HS-LDH.

| Atomic concentration (%) through XPS test | | | | | | | | | |
|---|------|------|------|------|-------|------|-------|-----|-------|
| Element | Ni | Co | Fe | Cu | C | N | O | Au | Ag |
| Value | 5.56 | 4.34 | 3.94 | 0.85 | 45.56 | 2.04 | 36.32 | 1.4 | trace |

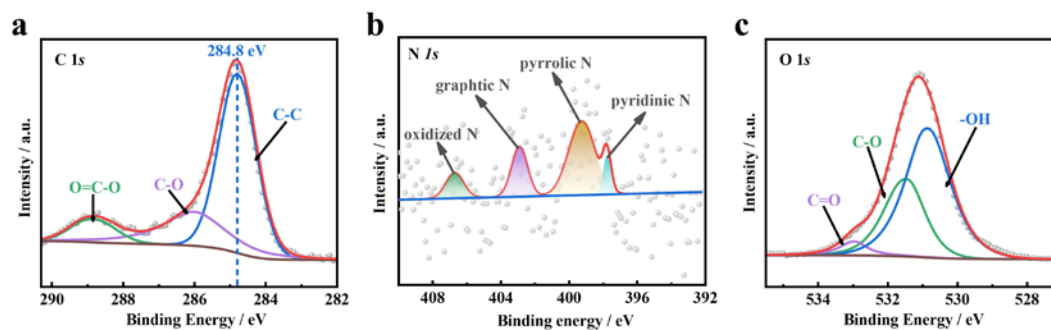


Figure S9. HR-XPS of C 1s, N 1s and O 1s of the NPG-HS-LDH.

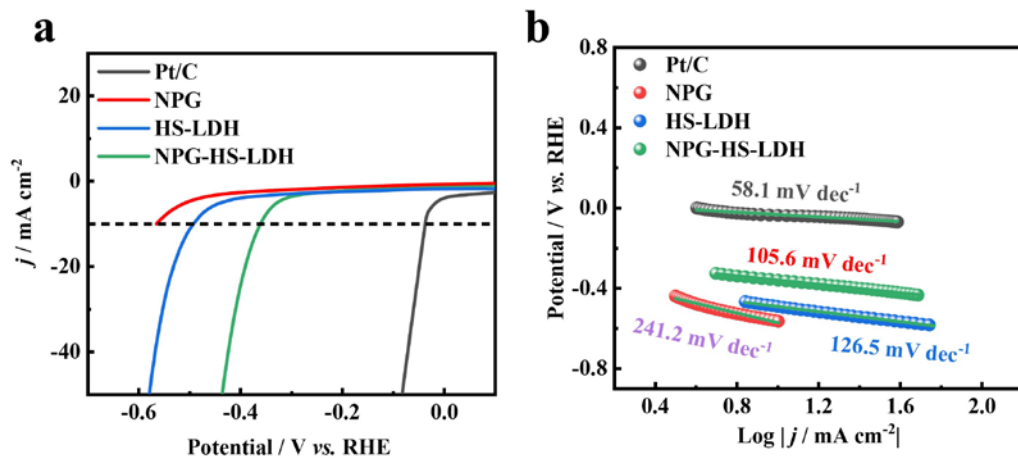


Figure S10. The HER performances of the NPG-HS-LDH and commercial Pt/C: (a) polarization curves; (b) the corresponding Tafel slopes.

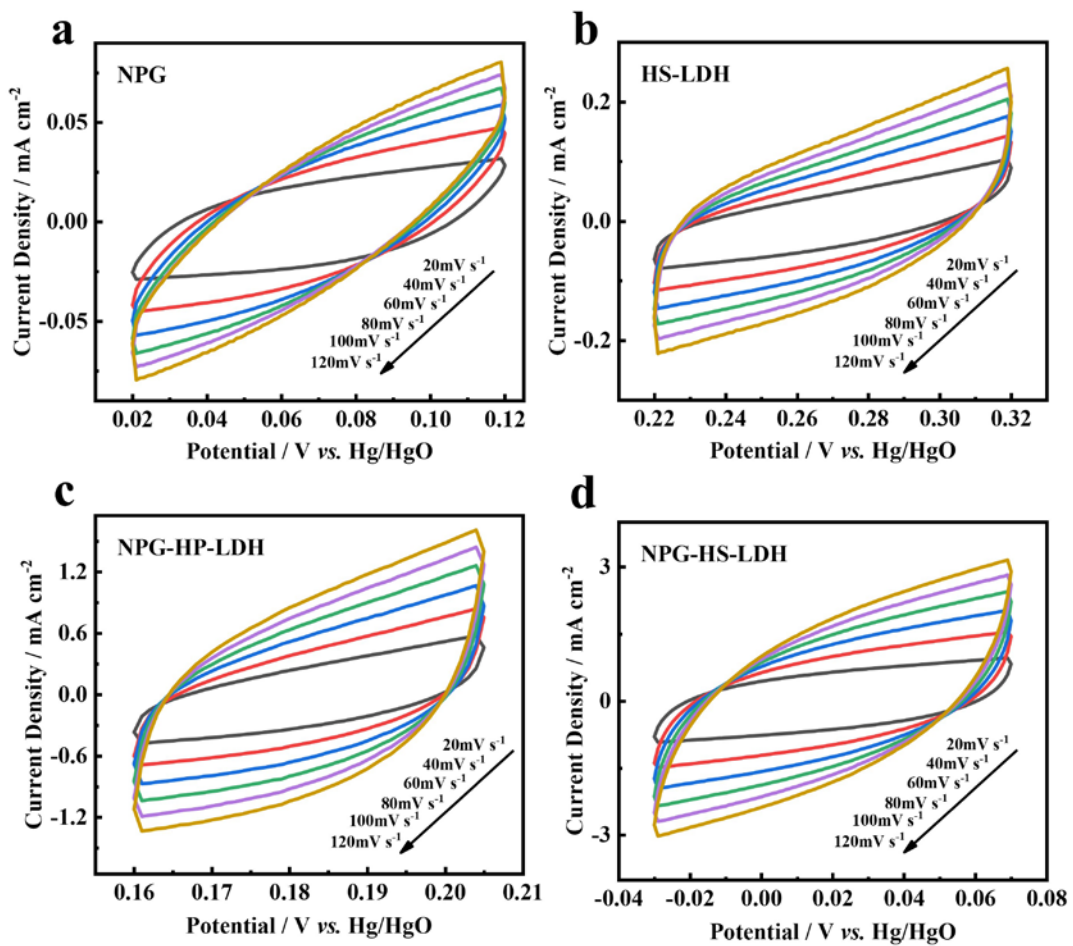


Figure S11. The electrochemical surface area (ECSA) tests of the as-prepared samples in 1 M KOH.

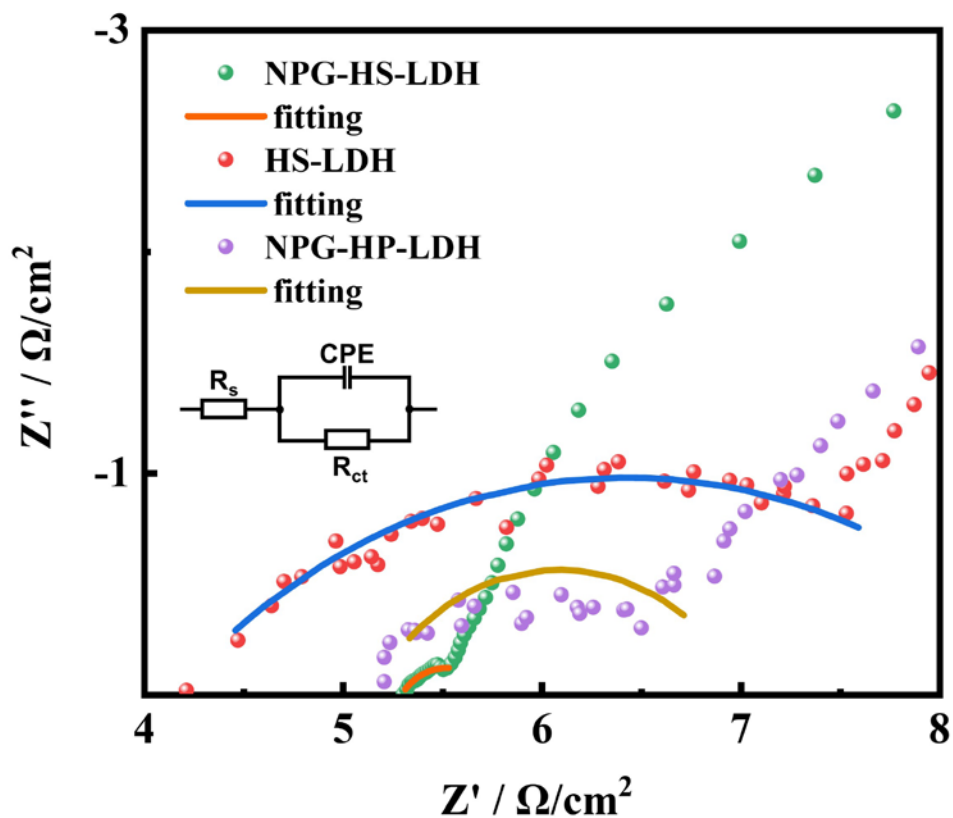


Figure S12. The EIS spectra of the as-prepared samples.

Table S3. R_s and R_{ct} values obtained through fitting of the EIS spectra.

| | NPG-HS-LDH | HS-LDH | NPG-HP-LDH |
|-------------------|------------|--------|------------|
| R_s / Ω | 5.297 | 4.146 | 5.148 |
| R_{ct} / Ω | 0.456 | 4.558 | 1.877 |

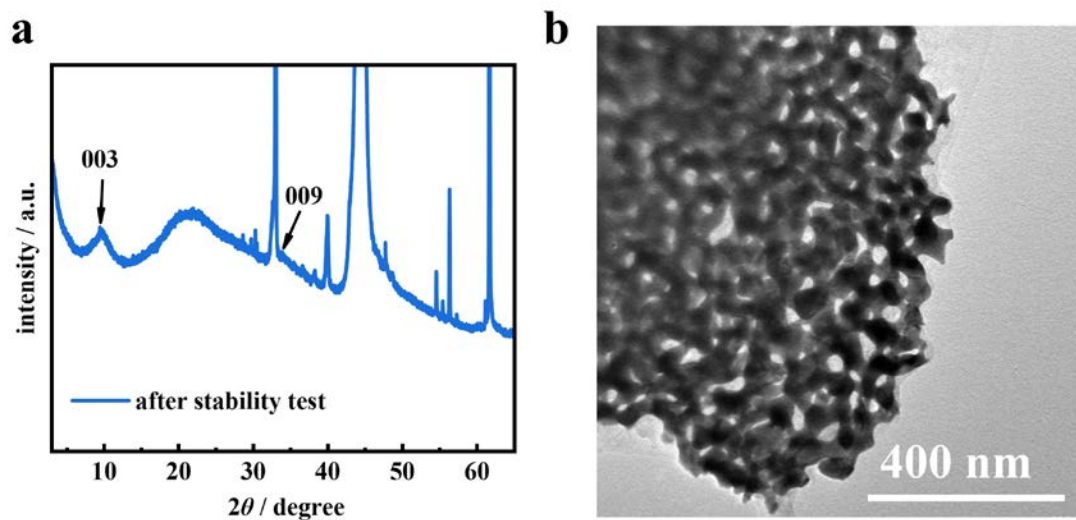


Figure S13. The XRD pattern (a) and TEM image (b) of the NPG-HS-LDH after stability test.

Table S4. Atomic concentration (at%) of each element presented in the XPS survey spectrum of the NPG-HS-LDH after stability test.

| Atomic concentration (%) after stability test via XPS | | | | | | | | | |
|---|------|------|------|------|-------|-----|------|-------|-------|
| Element | Ni | Co | Fe | Cu | C | N | O | Au | Ag |
| Value | 1.72 | 6.95 | 3.09 | 0.82 | 54.12 | 1.5 | 31.8 | trace | trace |

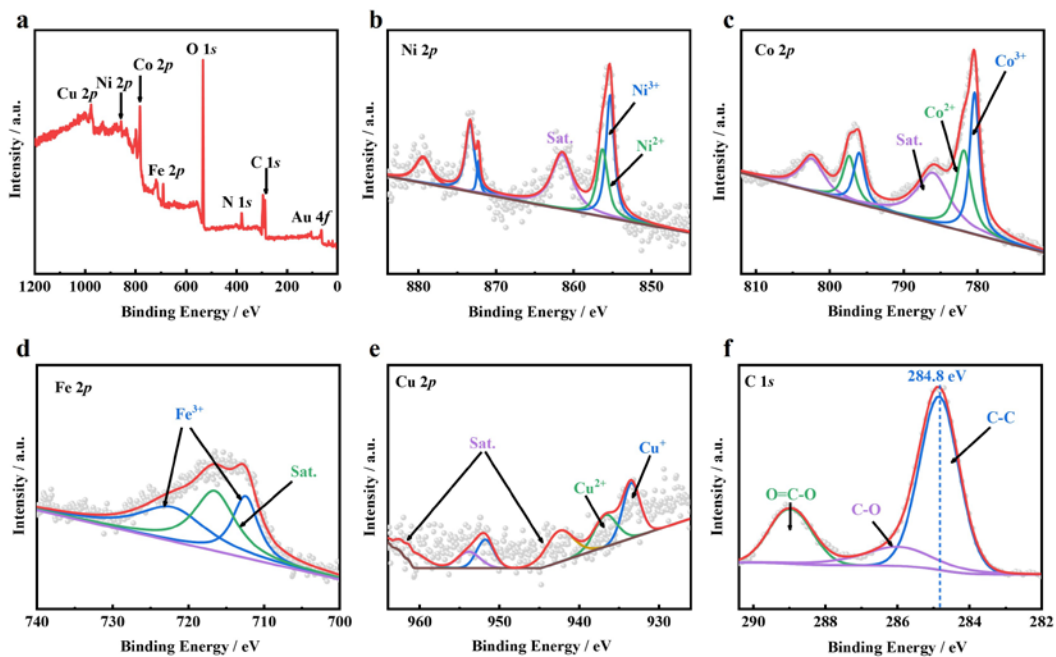


Figure S14. The XPS analysis of the NPG-HS-LDH after stability test.

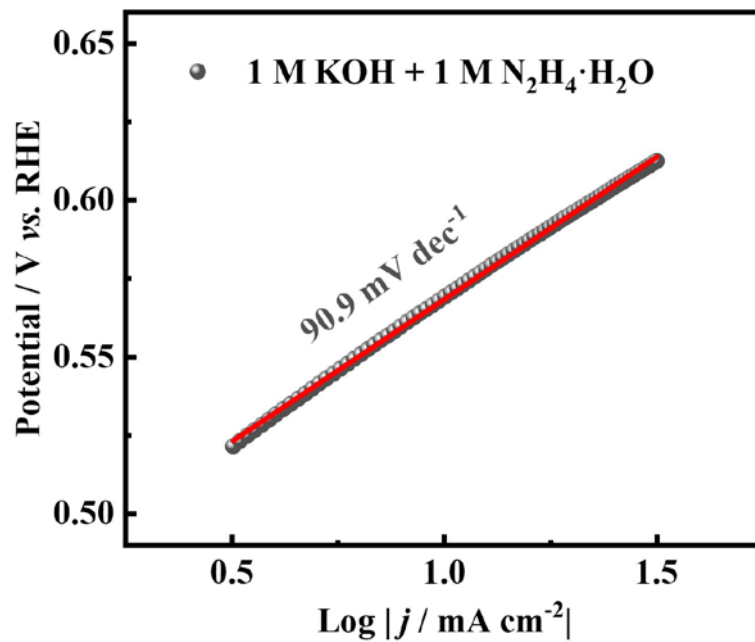


Figure 15. The corresponding Tafel slope of HzOR.